(27) Spectroscopic data has been collected for N_2 by D. C. Jain, *Int. J. Quantum Chem.*, **4**, 579 (1970), and for NO^+ by E. W. Thulstrup and Y. Ohrn, *J. Chem. Phys.*, **57**, 3716 (1972).
(28) J. H. Callomon and F. Creutzberg, *Proc. Int. Conf. Spectrosc., 1st, 1967*, 143–145 (1968); H. M. Rosenstock, *Int. J. Mass Spectrom. Ion Phys.*, **7**, 33 (1971).
(29) G. Herzberg, "Molecular Spectra and Molecular Structure. III. Electronic Spectra and Electronic Structure of Polyatomic Molecules", Van Nostrand-Reinhold, Princeton, N.J., 1966.
(30) L. C. Lorquet and C. Cadet, *Int. J. Mass Spectrom. Ion Phys.*, **7**, 245 (1971).
(31) R. K. Preston and J. C. Tully, *J. Chem. Phys.*, **54**, 4297 (1971).
(32) J. Tully, *J. Chem. Phys.*, **61**, 61 (1974).
(33) L. D. Landau, *Phys. Z. Sowjetunion*, **2**, 46 (1932).
(34) C. Zener, *Proc. R. Soc. London, Ser. A*, **137**, 696 (1932).
(35) E. E. Nikitin in "Chemische Elementarprozesse", H. Hartman, Ed., Springer-Verlag, West Berlin, 1968.
(36) M. Karplus, R. N. Porter, and R. D. Sharma, *J. Chem. Phys.*, **45**, 3871–3873 (1966).
(37) J. T. Muckerman, *J. Chem. Phys.*, **57**, 3388 (1972).
(38) R. F. Stebbings, B. R. Turner, and J. A. Rutherford, *J. Geophys. Res.*, **71**, 771 (1966).
(39) D. K. Bohme, P. P. Ong, J. B. Hasted, and L. R. Megill, *Planet. Space Sci.*, **15**, 1777 (1967).
(40) J. A. Rutherford and D. A. Vroom, *J. Chem. Phys.*, **55**, 5622 (1971).
(41) R. H. Neynaber and G. D. Magnuson, *J. Chem. Phys.*, **58**, 4586 (1973).
(42) G. P. K. Smith and R. J. Cross, Jr., *J. Chem. Phys.*, **60**, 2125 (1974).
(43) (a) Y. Kaneko, N. Kobayashi, and I. Kanomato, *Mass Spectrom.*, **18**, 920 (1970); (b) Y. Kaneko and N. Kobayashi, *J. Phys. Soc. Jpn.*, **36**, 1649 (1974).
(44) T. F. O'Malley, *J. Chem. Phys.*, **52**, 3269 (1970).
(45) J. R. Krenos, R. K. Preston, R. Wolfgang, and J. C. Tully, *J. Chem. Phys.*, **60**, 1634 (1974).
(46) M. L. Vestal and J. H. Futrell, *Proc. 22nd Annu. Conf. Mass Spectrom. Allied Topics*, (1974); private communication, May 1975.
(47) J. Berkowitz and J. H. D. Eland, *J. Chem. Phys.*, **67**, 2740–2752 (1977).
(48) H. S. Johnston, "Gas Phase Reaction Rate Theory", Ronald Press, New York, N.Y., 1966.
(49) R. J. Coleman, J. S. Delderfield, and B. G. Reuben, *Int. J. Mass Spectrom. Ion Phys.*, **2**, 25 (1969).
(50) J. Collin and F. P. Lossing, *J. Chem. Phys.*, **28**, 900 (1958).
(51) A. S. Newton and A. F. Sciamanna, *J. Chem. Phys.*, **44**, 4327–4332 (1966).
(52) V. H. Dibeler, J. A. Walker, and S. K. Liston, *J. Res. Natl. Bur. Stand., Sect. A*, **71**, 371 (1967).
(53) E. E. Ferguson, D. K. Bohme, F. C. Fehsenfeld, and D. B. Dunkin, *J. Chem. Phys.*, **50**, 5039 (1969).
(54) P. G. Orth and R. C. Dunbar, *J. Chem. Phys.*, **66**, 1616 (1977).

Force and Density Study on the Chemical Reaction Process $NH_2 + H \rightarrow NH_3$

H. Nakatsuji,* T. Koga, K. Kondo, and T. Yonezawa

Contribution from the Department of Hydrocarbon Chemistry, Faculty of Engineering, Kyoto University, Kyoto, Japan. *Received March 14, 1977*

Abstract: Force and density analysis for the radical reaction process $NH_2 + H \rightarrow NH_3$ is given on the basis of the electrostatic force (ESF) theory. We analyze the driving force acting on the approaching H nucleus during the reaction process and investigate the dynamic behavior of the electron cloud from the viewpoint of the electron cloud preceding and incomplete following. The results are: (1) In the initial stage of the reaction, the electron cloud preceding in the atomic region of H, i.e., the inward polarization of the electron cloud, is dominant. The resultant atomic dipole (AD) force gives the predominant contribution to the driving force. However, the stabilization energy due to this AD force is small. (2) In the intermediate stage, the electron cloud preceding occurs as a flow of electron density into the N–H overlap region from the region behind the approaching H nucleus. The electron density thus accumulated in the N–H region gives a large attractive exchange (EC) force. This EC(H–N) force is the dominant driving force of the reaction and gives a predominant contribution to the stabilization energy (heat of reaction) of the system. (3) In the last stage, the repulsive extended gross charge (EGC) force between the undershielded nuclei increases rapidly and terminates the reaction. (4) The addition of the polarization function on the H atom is important to improve the Hellmann–Feynman (H–F) force acting on the H nucleus in the initial and intermediate stages.

Introduction

During the last decade, several force and density studies on the chemical reaction processes have appeared[1,2] on the basis of the electrostatic Hellmann–Feynman (H–F) theorem,[3]

$$\mathbf{F}_A = Z_A \left[\int (\mathbf{r}_{A1}/r_{A1}^3)\rho(\mathbf{r}_1)\, d\mathbf{r}_1 - \sum_{B(\neq A)} Z_B \mathbf{R}_{AB}/R_{AB}^3 \right] \quad (1)$$

which permits us a simple interpretation of the force through semiclassical electrostatics. Bader and Chandra[4] studied the reaction process $H + H \rightarrow H_2$, analyzing in detail the H–F force and the behaviors of the electron density along the process. They also examined the repulsive He_2 system and compared it with the H_2 system. Chandra and Sunder[5] reported a similar analysis for the formation of the Li_2 molecule and discussed the roles of the core and valence electron densities for the force acting on the nucleus. Nakatsuji, Kuwata, and Yoshida[7] studied the dimerization reaction of two methyl radicals on the basis of the elerostatic force (ESF) theory.[6-9] They have shown that the geometrical change of the reactant, which is induced by the interaction, would be very importart for the occurrence of this reaction. Fukui, Kato, and Fujimoto[10] have studied the reaction coordinate for the substitution reaction $CH_4 + T \rightarrow CH_3T + H$, and analyzed the H–F force in terms of the conventional perturbation theoretic approach to chemical reactions.[11] Curtiss, Kern, and Matcha[12] have calculated the electron density maps for several diatomic alkali halides and analyzed them in relation to the binding and antibinding diagram due to Berlin.[13] Chandra and Sebastian[14a] have recently reported a force analysis for the reaction $He^+ + He^+ \rightarrow He_2^{2+}$, which showed a similar behavior to the previous H_2 system.[4] They have also studied the reactions $He + H^+/He^+ + H \rightarrow HeH^+$.[14b]

Alternatively, we have developed the electrostatic force (ESF) theory for a molecule and interacting molecules and applied it to molecular structures, chemical reactions, and long-range forces.[6-9] In the ESF theory, we have partitioned the H–F force into three pictorial components: atomic dipole (AD) force, exchange (EC) force, and extended gross charge (EGC) force. This partitioning is convenient since they are closely related with the chemical intuitions such as lone pair, bond, and gross charge, respectively. Bader and Jones[15] gave

0002-7863/78/1500-1029$01.00/0

earlier a similar partitioning but it is different from the above one.[8] Starting from this partitioning, we have developed the ESF theory, which has been shown to be quite successful, especially in understanding and predicting various molecular structures and some of the chemical reactions.[6,7] It has also been applied to the analyses of long-range forces.[9] The basic concept of the ESF theory is common to all of these phenomena.

Due to the H-F theorem, the forces acting on the nuclei of a system undergoing a nuclear rearrangement process are determined by the behavior (reorganization) of the electron density $\rho(\mathbf{r}_1)$ under the process. Such behaviors of electron density have been investigated by several authors,[16] especially in relation to molecular vibrations. Previously, one of the authors has studied such behaviors from a more general point of view and shown that the two general behaviors of the electron density, the electron cloud preceding and/or the electron cloud incomplete following, should commonly occur in *any* nuclear rearrangement processes.[8] The former means the behavior that the centroid of the local electron cloud near the moving nucleus precedes the nuclear position in the direction of the rearrangement coordinate. It works to accelerate the nuclear rearrangement process, i.e., the preceded electron cloud pulls the nucleus in the direction of the process. The latter means just the reverse behavior and works to resist the nuclear rearrangement process. These behaviors and roles of the electron density have been observed in various molecular processes[3b,4,5,7,8,9a,16] and are shown to be closely related to the ESF theory.[8] Such density analysis has also given a general guiding principle for the nuclear rearrangement processes on the basis of the electron density behaviors of the system.[6b,8]

In this article, we study the force and density aspect of the radical reaction process $NH_2 + H \rightarrow NH_3$ with the use of the ESF concept. The electron density was calculated with the multiconfigurational (MC) SCF method[17] constructed from the localized molecular orbitals (LMOs).[18] The basis set used was the minimal STO-3G basis plus p-type polarization functions on each hydrogen atom. As is well known,[19] the problem in the H-F force calculation is that the force is sensitive to the inaccuracies of the wave function if it does not satisfy the variational condition such as the floating or the stable condition.[20,21] However, since such inaccuracy is due mainly to the inaccuracy in the electron density in the local atomic region, the addition of the polarization function considerably improves the H-F force.[22] Then, we have added p-type polarization functions on the H atoms in order to improve the forces acting on the H nuclei. However, at this level of basis set, the H-F force acting on the nitrogen nucleus is still very crude, so that we have limited ourselves to analyze only the force acting on the H nuclei. In the next section, we briefly summarize the computational method and discuss the accuracy of the calculated H-F forces. Then, we give the force and density analyses of the reaction process. We investigate the roles of the AD, EC, and EGC forces in the reaction process and the dynamic behaviors of the electron cloud along the process in the viewpoint of the electron cloud preceding and following. The summary of the present study will be given in the last section.

Computational Method

A. Partitioning of the H-F Force. Expanding the one-electron density $\rho(\mathbf{r}_1)$ in eq 1 by a suitable set of atomic orbitals (AOs) $\{\chi_r\}$,

$$\rho(\mathbf{r}_1) = \sum_{r,s} P_{rs}\chi_r(\mathbf{r}_1)\chi_s(\mathbf{r}_1) \tag{2}$$

we partition the H-F force given by eq 1 into atomic dipole (AD), exchange (EC), and extended gross charge (EGC) forces. That is,

$$\mathbf{F}_A = \mathbf{F}_A^{AD} + \mathbf{F}_A^{EC} + \mathbf{F}_A^{EGC} \tag{3}$$

where

$$\mathbf{F}_A^{AD} = Z_A \sum_r^A \sum_s^A P_{rAsA} \langle \chi_{rA} | \mathbf{f}_A | \chi_{sA} \rangle \tag{4a}$$

$$\begin{cases} \mathbf{F}_A^{EC} = \sum_{B(\neq A)} \mathbf{F}_A^{EC}(AB) \\ \mathbf{F}_A^{EC}(AB) = 2Z_A \sum_r^A \sum_s^B P_{rAsB} \langle \chi_{rA} | (\mathbf{f}_A)_0 | \chi_{sB} \rangle \end{cases} \tag{4b}$$

$$\begin{cases} \mathbf{F}_A^{EGC} = \sum_{B(\neq A)} \mathbf{F}_A^{EGC}(AB) \\ \mathbf{F}_A^{EGC}(AB) = Z_A \sum_r^B \sum_s^B P_{rBsB} \langle \chi_{rB} | \mathbf{f}_A | \chi_{sB} \rangle \\ \qquad + Z_A \sum_r^A \sum_s^B P_{rAsB} S_{rAsB} \langle \chi_{sB} | \mathbf{f}_A | \chi_{sB} \rangle \\ \qquad + Z_A \sum_{C(\neq A,B)} \sum_r^B \sum_s^C P_{rBsC} \langle \chi_{rB} | \mathbf{f}_A | \chi_{sC} \rangle \\ \qquad - Z_A Z_B \mathbf{R}_{AB}/R_{AB}^3 \end{cases} \tag{4c}$$

Here, $\mathbf{f}_A$ means $\mathbf{r}_{A1}/r_{A1}^3$, P_{rs} and S_{rs} the bond order-density and overlap integral between χ_r and χ_s, and Σ_r^A the summation over the AOs belonging to the atom A.

The physical meanings of the AD, EC, and EGC forces are as follows.[6] The atomic dipole (AD) force represents the attraction exerted on the nucleus A from the centroid of the polarized electron cloud near the nucleus A. The most frequent example of such polarized atomic density is found for the lone-pair electron density on atom A. The exchange (EC) force is the attraction (or repulsion) due to the electron cloud which is accumulated (or excluded) in the overlap region between atoms A and B. In eq 4b, the net-exchange force integral $\langle \chi_{rA} | (\mathbf{f}_A)_0 | \chi_{sB} \rangle$ is defined by

$$\langle \chi_{rA} | (\mathbf{f}_A)_0 | \chi_{sB} \rangle \equiv \langle \chi_{rA} | \mathbf{f}_A | \chi_{sB} \rangle - \frac{1}{2} S_{rAsB} \langle \chi_{sB} | \mathbf{f}_A | \chi_{sB} \rangle \tag{5}$$

where the second term subtracts from the first term the effect that the bond electron cloud shields the nuclear charge Z_B.[6a] Such effect is included in the EGC force. The extended gross charge (EGC) force represents the interaction of the nucleus A with the nucleus B which is shielded by the surrounding electron cloud. All the AD, EC, and EGC forces are well defined and add up to the H-F force which is referred to as the total force in the text. We note that this partitioning of the H-F force is connected directly[8] to the partitioning of the electron density into the interference and quasi-classical densities which are shown by Ruedenberg[23] to represent adequately the density reorganization in molecular formation processes. This is not true, however, for the partitioning proposed by Bader et al.[15]

B. Computational Detail and Accuracy. Experimental geometry, i.e., bond length N-H = 1.0173 Å and valence angle ∠HNH = 107.8°,[24] is used for the equilibrium NH_3 molecule. The geometry of the NH_2 fragment of the system is assumed to be fixed throughout the reaction process. This would be a reasonable approximation since NH_2 and NH_3 have similar bond lengths and valence angles (N-H = 1.024 Å and ∠HNH = 103.4° for NH_2).[24]

The required electron density was calculated by the MCSCF method.[25,26] Two configurations, $(1s)^2\sigma^2\sigma^2n^2\sigma^2$ and $(1s)^2\sigma^2\sigma^2n^2\sigma^{*2}$, were chosen where the last σ and σ^* orbitals mean the bonding and antibonding LMOs of the forming N-H bond. This wave function gives a reasonable asymptotic behavior at the dissociation limit into NH_2 radical and H atom (see Figure 2).

Table I. Comparison of the H-F Force and Energetic Results[a]

	H-F force	Energetics	Exptl
Equilibrium bond length, Å	1.12	1.06	1.0173[b]
Force constant, mdyn/Å	7.19	10.32	7.052[c]
Heat of reaction, kcal/mol			
until 2.0 Å	21.5	22.5	
until 1.6 Å	47.2	56.0	
overall	74.4	110.4	101[d]

[a] The extended basis set was used. [b] Reference 24. [c] Reference 30. [d] Reference 24.

Table II. Effect of the Addition of the p-Type Polarization Functions ($\zeta = 0.25$) on the H-F Force Acting on the H Nucleus[a]

	With p's	Without p's
MCSCF energy	−55.4379	−55.3794
AD force[b]	−0.0033	0.0
EC(H-N) force	−0.0653	−0.0767
EC(H···H) force	−0.0083	+0.0065
EGC force	+0.0197	+0.0270
Total force	−0.0572	−0.0432

[a] Calculations were carried out at $R = 1.6$ Å on the reaction path. All values are given in atomic unit. [b] The positive and negative signs mean repulsive and attractive forces, respectively.

We have first calculated the minimum energy reaction path (Figure 1) with the minimal STO-3G basis of Stewart[29] having the Slater-rule exponents except for $\zeta_H = 1.2$. Then, we have recalculated the wave functions along the obtained path using the extended basis set which includes 1G p-type polarization functions on the three hydrogen atoms. The exponent of the additional p functions was determined variationally to be 0.25 for the equilibrium NH_3 geometry.

In Table I, we have compared several quantities obtained from the H-F force, energetics, and experiment in order to examine the accuracies of the H-F force and the basis set used. The H-F force results for the equilibrium bond length and force constant are comparable with the experimental values. This suggests that the calculated H-F force is reasonable near the equilibrium geometry. The stabilization energies of the system have been calculated at two intermediate (N-H = 2.0, 1.6 Å) and the equilibrium structures by the numerical integration of the H-F force along the reaction path (Figure 3). The obtained energies are 96% of the energetic result for the range ∞-2.0 Å and 84% for ∞-1.6 Å. The heat of reaction, i.e., the overall stabilization energy, is about 70% of the energetic and experimental values. These results indicate that the calculated H-F forces are smaller than the corresponding energy gradients only in the intermediate stage of the reaction. This was also confirmed by comparing the H-F force with the numerical derivative of the energy.

The addition of the polarization function is important to improve the H-F force.[22] When the minimal STO-3G basis was used, the heat of reaction was only ~40% of the experimental value. Table II compares the H-F forces calculated by the minimal and extended basis sets. Although the effect of polarization function is small for the MCSCF energy, it is large for the H-F force. The polarization functions give rise to the attractive AD force and decrease the repulsive EGC force. The attractive EC(H-N) force slightly decreases and the EC(H···H) force changes from repulsive to attractive. The sum of these effects is to increase the attractive total force by the amount of ~30%. Thus, the polarization function is important for the H-F force and we have used the extended basis set in the present calculations.

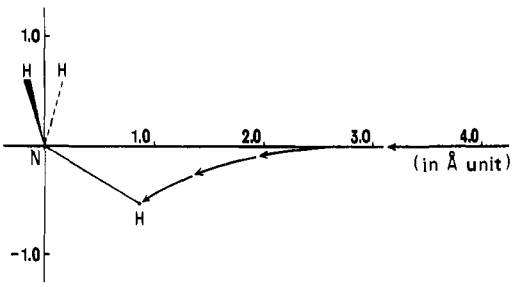

Figure 1. The calculated minimum energy path for the reaction $NH_2 + H \rightarrow NH_3$.

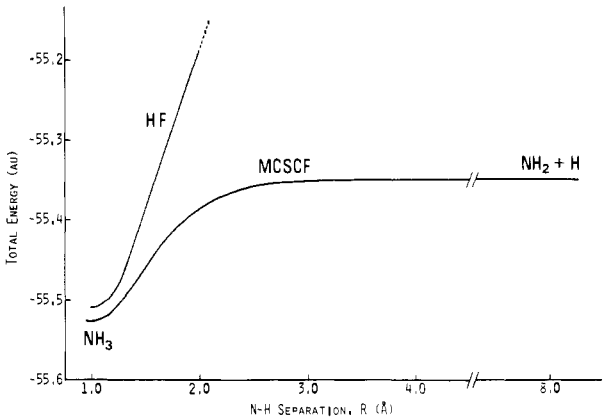

Figure 2. The potential energy curves for the reaction $NH_2 + H \rightarrow NH_3$ along the reaction path.

Results and Discussion

A. Reaction Path and Potential Energy Curve. The minimum energy reaction path was calculated as shown in Figure 1. Although this reaction path was determined from the MCSCF energy, we have confirmed that the calculated H-F force also gives the reaction path very close to that given in Figure 1. In the initial stage, the hydrogen atom approaches the NH_2 radical in the perpendicular direction to the NH_2 plane, and attacks the $p\pi$-type radical orbital of NH_2. As the reaction proceeds, the hydrogen gradually turns downward and results in the equilibrium C_{3v} geometry of ammonia molecule. From this reaction path, we may expect the possibility of the rotational excitation of the NH_2 fragment, when NH_3 molecule is dissociated into NH_2 radical and H atom.

Figure 2 shows the potential energy curves calculated by the Hartree-Fock and the MCSCF methods as a function of the N-H distance, R, along the reaction path. Both curves were obtained with the extended basis set. The addition of the polarization function lowered the energy of the system by ~0.06 au. For $R > 2$ Å, the Hartree-Fock method did not converge, while the present MCSCF method has given a reasonable asymptotic behavior at the dissociation limit. From Figure 2, it is seen that there is no activation barrier for this reaction. The calculated heat of formation of the N-H bond is 110.4 kcal/mol, which is slightly larger than the experimental value of 101 kcal/mol.[24]

B. Force along the Reaction Path. The force acting on the nucleus of the approaching hydrogen atom is shown in Figure 3 as a function of R. We plot the force component parallel to the N-H axis, i.e., the force which changes the N-H distance. The positive and negative signs mean the repulsive and attractive forces, respectively. The total force gradually becomes attractive from $R \simeq 3.5$ Å. Near 1.5 Å, the total driving force reaches its maximum attraction which corresponds to the change in curvature of the potential energy curve (Figure 2). Then, the attractive force decreases rapidly and the system

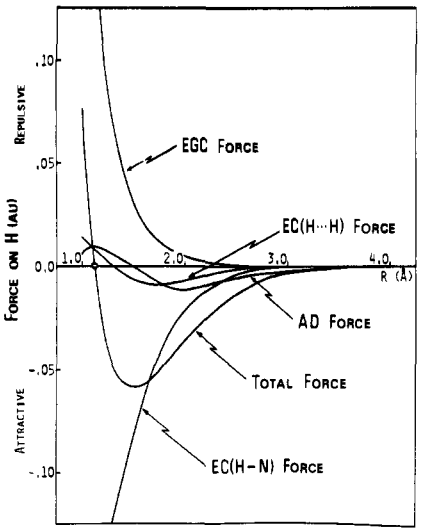

Figure 3. The force acting on the approaching H atom. The force component parallel to the N-H axis is plotted as a function of the N-H separation, R.

Table III. Transverse Force Acting on the H Nucleus of the NH_2 Fragment in the NH_2 Plane[a]

R, Å	F_H, au
1.1[b]	+0.0005
1.3	−0.0033
1.6–8.0	−0.0050

[a] The positive and negative forces work to increase and decrease the HNH angle, respectively. [b] Near the equilibrium bond length, 1.12 Å.

reaches the equilibrium geometry where the total force vanishes (marked by open circle in Figure 3). The calculated N-H bond distance is 1.12 Å, which is somewhat larger than the experimental bond length 1.0173 Å.[24] At the calculated equilibrium geometry, the quadratic N-H stretching force constant has been calculated to be 7.19 mdyn/Å. This value is comparable with the experimental value 7.052 mdyn/Å,[30] whereas the energetics has given 10.32 mdyn/Å. The corresponding value obtained with the STO-3G basis set was reported to be 10.791 mdyn/Å.[31]

Table III shows the transverse force acting on the H nucleus of the NH_2 fragment in the NH_2 plane. For $R \geq 1.6$ Å, a small force has been obtained which works to decrease the HNH angle, but in the range $1.6 > R > R_e$, the force gradually decreases and vanishes near the equilibrium distance. This agrees with the experimental difference in the valence angles of NH_3 (107.8°) and NH_2 (103.4°), since the HNH angle of the NH_2 fragment has been fixed, in the present calculation, to that of the NH_3 throughout the reaction.

Next, we analyze the driving force of the reaction in terms of the AD, EC, and EGC forces. In the initial stage of the reaction ($R > 3$ Å), only the attractive AD force is dominant which is caused by the inward polarization of the electron cloud near the H atom. Such trend was also found by Bader and Chandra for the reaction $2H \rightarrow H_2$.[4] Further, it has been shown[3b,9a,32] that the van der Waals forces between two neutral S-state atoms also originate from such kind of inward polarization of electron cloud and the resultant AD force. These results suggest that for reactions between neutral reactants, the AD force would be the most important origin of the driving force until a moderately long-range separation. In the present reaction, the predominance of the AD force continues until $R \simeq 2.4$ Å. In the shorter region than $R = 2.4$ Å, the attraction due to the EC(H-N) force, which means the EC force due to the electron cloud in the H-N overlapping region, becomes the dominant origin of the driving force of the reaction. It reflects a rapid accumulation of the electron density in the H-N region and shows a shorter range character of the EC(H-N) force than the AD force. Such predominance of the EC force in the intermediate stage was also reported previously for the reactions $2H \rightarrow H_2$[4] and $2CH_3 \rightarrow C_2H_6$,[7] so that this would be common to radical reactions. As shown in the next section, these roles of the AD and EC forces are the results of the electron cloud preceding in the course of the reaction. The EC(H···H) force due to the electron cloud between the nonbonded hydrogens gives a small but attractive contribution until $R \simeq 1.3$ Å. The attractive character of this force may be understood from the fact that the attacking hydrogen is an open-shell radical. The EGC force gives a repulsive contribution from ~3 Å, and increases rapidly for $R < 1.5$ Å and terminates the reaction at $R = 1.12$ Å. Near the equilibrium bond length, the AD and EC(H···H) forces also become repulsive, but their contributions are relatively small. This repulsive AD force suggests the occurrence of the electron cloud incomplete following near the H nucleus in the last stage of the reaction. The repulsion of the EC(H···H) force may be due to the interaction between the doubly occupied N-H bond orbitals (exchange repulsion) as seen in the He-He system.[4]

It is interesting to note that the overall trend found here for the $NH_2 + H$ system is similar to that found for the simpler $H + H$ system,[4] so long as we look upon the force acting on the approaching hydrogen atom. Though we expect that such similarity would hold more generally for the radical reactions including hydrogen atoms, more extensive studies would be necessary for the final conclusion.

The integration of the H-F force along the reaction path gives a different analysis of the stabilization energy from the conventional energetic ones. Table IV shows the partitioning of the stabilization energy into the AD, EC(H-N), EC(H···H), and EGC components. This partitioning has been obtained by the numerical integrations of the respective force curves. In the initial stage (∞–2.4 Å), the stabilization energy is mainly due to the AD force (68%) caused by the polarization of the atomic electron density. However, the stabilization energy due to this density behavior (4.0 kcal/mol) is much smaller than the overall stabilization energy (74.4 kcal/mol). For the stabilization energy up to $R = 1.53$ Å (initial and intermediate stages), the EC(H-N) force gives a dominant contribution

Table IV. Partitioning of the Stabilization Energy into the AD, EC, and EGC Components[a,b]

	ΔE		
	Initial (∞–2.4 Å)	Initial and intermediate (∞–1.53 Å)	Overall (∞–equilibrium (1.12 Å))
AD	4.0 (68)	14.0 (29)	11.9 (16)
EC(H-N)	1.5 (25)	36.0 (73)	97.5 (131)
EC(H···H)	0.6 (10)	8.4 (17)	8.1 (11)
EGC	−0.2 (−3)	−9.3 (−19)	−43.1 (−58)
Total	5.9 (100)	49.1 (100)	74.4 (100)

[a] Energies are in kcal/mol. Values in parentheses are percent ratios. [b] At 2.4 Å, the AD and EC(H-N) forces give equal contributions to the driving force. At 1.53 Å, the total driving force reaches its maximum attraction and at 1.12 Å the total force vanishes.

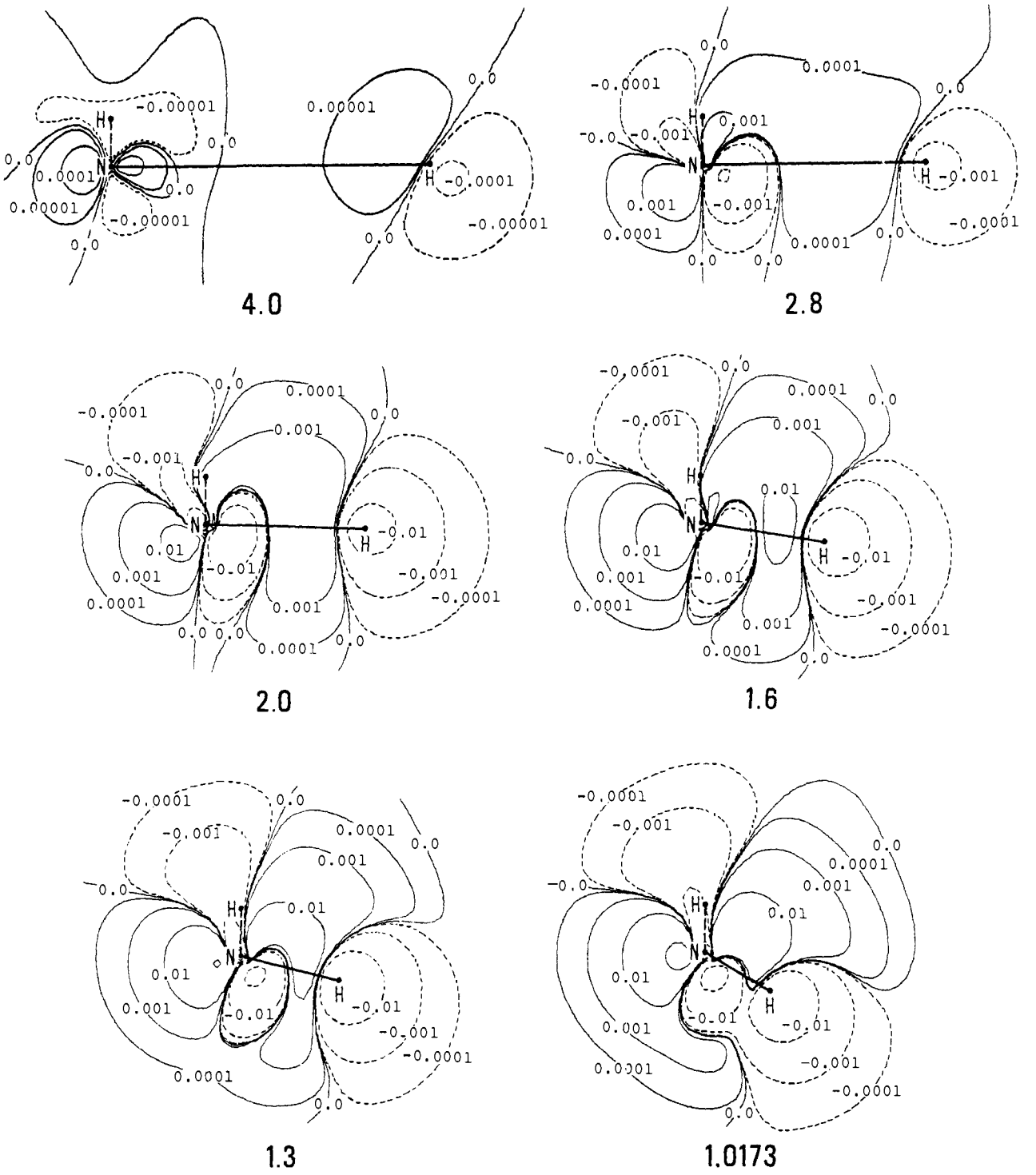

Figure 4. The density difference $\Delta\rho$ contour maps (au) for the NH_2–H system at several N–H separations. Solid lines and positive values mean the increase in the electron density relative to the separated system, while dashed lines and negative values the decrease in the electron density. The N–H distances indicated below the maps are given in Å unit.

(73%). This is also true for the overall stabilization energy (heat of reaction) (131%), showing that this EC(H–N) force is the most important origin of the stabilization energy. Namely, the accumulation of the electron density in the H–N overlap region is the predominant density origin of the heat of reaction. This would be true more generally for radical reactions. The EGC force contributes to destabilize the system throughout the reaction. The effect rapidly increases in the last stage (−43.1 kcal/mol), and cancels about one-half of the stabilization energy due to the EC(H–N) force. Despite the importance of the AD force in the initial stage, its contribution to the heat of reaction is rather small (16%). The EC(H···H) force also gives a small but stabilizing contribution (11%). We note that the above analysis of the stabilization energy is completely different from the conventional energetic one and is based *only* on the electron density of the system. It gives a direct way to connect the dynamic behavior of the electron cloud (e.g., electron cloud preceding discussed in the next section) with the stabilization energy of the system.

C. Dynamic Behavior of Electron Cloud. In this section, we study the density origin of the reaction by investigating the dynamic behavior of the electron cloud during the reaction process. As reported previously,[8] the electron cloud preceding and/or the electron cloud incomplete following are expected

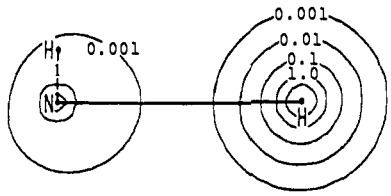

2.8

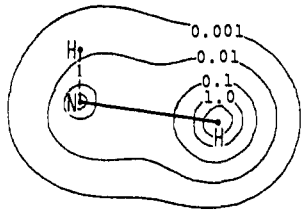

1.6

Figure 5. The weighted density ω_H contour maps for the approaching H nucleus. The contour values are given in au, while the N-H distances are in Å unit.

to occur during any nuclear rearrangement processes. For the present reaction, the electron cloud preceding would occur until the reaction is completed ($R = \infty - R_e$), since the reaction proceeds monotonously without energy barrier and with an increase in nuclear repulsion.[8] In the following, we analyze these behaviors of electron cloud using the density difference maps $\Delta\rho(\mathbf{r})$, the weighted density maps $w(\mathrm{r})$, and the localized MO (LMO) maps.

The density difference $\Delta\rho$ is defined as the change in the electron density as the NH_2 and H radicals approach each other.

$$\Delta\rho = \rho(NH_2\text{-}H) - [\rho(NH_2) + \rho(H)] \qquad (6)$$

The $\Delta\rho$ maps are shown in Figure 4 for various values of R along the reaction path. We have used the density at 8.0 Å as the reference density $[\rho(NH_2) + \rho(H)]$. Figure 4 shows the typical features of the electron cloud preceding. At 4.0 Å, the electron cloud near the H atom is polarized inwardly, which is just the electron cloud preceding in the atomic region. As discussed in the preceding section, this is the origin of the attractive AD force important in the initial stage. As the internuclear separation decreases (R = 2.8–1.3 Å), the electron cloud preceding occurs as a flow of the electron cloud into the N-H overlap region from the region behind the approaching H nucleus. The electron density thus preceding the nuclear position pulls the H nucleus in the direction of the reaction process. This is the origin of the attractive EC(H-N) force, which is the most important driving force of the reaction for $R < 2.4$ Å, and which is the dominant origin of the heat of the reaction. Such features of electron-cloud reorganization have also been found for some simple reactions,[4,5,7,14] and may indicate the covalent character[33a] of the reaction. At the equilibrium geometry, the electron density increases within the two cones made of the three N-H axes and their extensions. It works to cancel the internuclear repulsion to keep a pyramidal shape. During the reaction, a d-type polarization[33b] of electron cloud is seen in the neighborhood of the N nucleus. The increase in the electron cloud in the left-hand side of the N nucleus is due to the rotation of the lone pair density from the lone pair of NH_2 to that of NH_3. This point will be seen later in the LMO maps.

Bader et al.[33] have analyzed the $\Delta\rho$ maps for many diatomic molecules at their equilibrium bond lengths. They have shown that the reorganization of electron density in the atomic region is p type in nature when an atom employs s orbitals in its bonding, while it is d type when an atom employs p orbitals.[33b] This is also confirmed in the present study not only for the equilibrium structure but for every stage of the reaction; i.e., in Figure 4, all the $\Delta\rho$ maps show a p-type polarization near the approaching H nucleus ("bonding" p type[4] which is the electron cloud preceding) and a d-type one near the N nucleus. The present $\Delta\rho$ map for the equilibrium NH_3 molecule may be directly compared with that of the diatomic NH molecule studied by Bader, Keaveny, and Cade.[33c] For the NH molecule, the electron density is accumulated in the two regions along the N-H axis: the region between N and H nuclei and the backward region of N. In the equilibrium NH_3 molecule, however, the electron density increases along the C_{3v} axis rather than the newly formed N-H bond: the lone-pair region of N and the pyramidal region within the three N-H bonds (see the $\Delta\rho$ map for R = 1.0173 Å in Figure 4). The latter may reflect the bent bond character[8] of the N-H bonds at the equilibrium pyramidal shape of NH_3. Thus, in polyatomic molecules, the p-type and d-type polarizations are rotated around the respective atoms in accordance with the symmetry of the molecule and the roles of the reorganized electron density.

Next, we investigate the dynamic behavior of the electron cloud using the weighted density $\omega_A(\mathbf{r}_1)$, which is defined by

$$\omega_A(\mathbf{r}_1) = \frac{1}{r_{A1}^3}\rho(\mathbf{r}_1) \qquad (7)$$

Using this quantity, the H-F force is rewritten as

$$\mathbf{F}_A = Z_A\left[\int \mathbf{r}_{A1}\omega_A(\mathbf{r}_1)\mathrm{d}\mathbf{r}_1 - \sum_{B(\neq A)} Z_B\mathbf{R}_{AB}/R_{AB}^3\right] \qquad (8)$$

Namely, the electronic part of the H-F force is proportional to the vector pointing from the nucleus A to the centroid of the weighted density $\omega_A(\mathbf{r}_1)$. For the present reaction, the H-F force $\mathbf{F}_A$ is always attractive until the reaction completes and the nuclear part is repulsive throughout the process. Therefore,[8] we expect that the centroid of the weighted density should always precede the position of the attacking hydrogen nucleus. This is a precise concept from which the approximate concept of the electron cloud preceding has been deduced.[8]

The weighted density maps at R = 2.8 and 1.6 Å are shown in Figure 5. At 2.8 Å, the map is composed of two spherical distributions near the H and N nuclei, corresponding to a very small accumulation of the electron cloud in the N-H region (small EC(H-N) force). The contribution of the sphere around the H nucleus is larger than that of the N nucleus. By checking the fine details, we can see that the sphere around the H is slightly polarized in the direction of the N nucleus. This is the weighted density preceding in the atomic region and the origin of the attractive AD force. At R = 1.6 Å, the weighted density accumulates also in the N-H region, showing the importance of the EC(H-N) force. The centroid of this contour lies somewhere *on* the N-H axis between the H and N nuclei. This is the preceding of the weighted density into the interatomic region. Throughout the process, such preceding of the weighted density has been confirmed, and further it was found that the weighted density maps are almost symmetric about the N-H axis as seen in Figure 5. Then, the electronic part of the H-F force on the H nucleus is always attractive and points *toward* the N nucleus.[34]

The behaviors of the N-H bond and lone-pair electron densities during the reaction process may be conveniently represented by their LMO maps. Figure 6 shows the maps for the N-H bond at 4.0 and 1.6 Å. Although the N-H bond LMO at R = 8.0 Å was simply the sum of the independent pπ AO

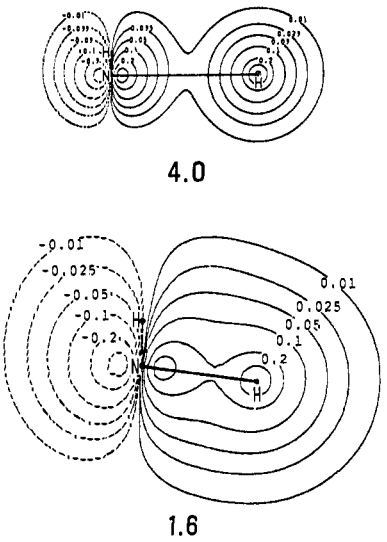

Figure 6. The N-H bond LMO maps. The contour values are given in au, while the N-H distances are in Å unit. The map for 4.0 Å is drawn in 1/2 scale relative to the map for 1.6 Å.

on NH_2 and 1s AO on H, the LMO at $R = 4.0$ Å still has such character. However, the N-H bond LMO at 1.6 Å already shows a typical pattern of the bonding LMO.

Figure 7 shows the maps for the lone-pair LMOs. Until 2.8 Å, the lone-pair LMO is quite insensitive to the reaction process and continues to be essentially the lone-pair orbital of the free NH_2 radical. In the shorter range, however, the long-pair LMO bends toward the C_{3v} axis of the equilibrium NH_3 molecule without much changing its contours.[35] The bending has occurred remarkably between $R = 1.3$ and 1.0173 Å (equilibrium structure). In a previous study for the dimerization reaction of two methyl radicals,[7] $2CH_3 \rightarrow C_2H_6$, it has been shown that the bending of the C-H bonds (i.e., planar to pyramidal) would be important for the occurrence of the reaction. The present situation resembles this case in that the three valence electron pairs of NH_2, two bond pairs and one lone pair, change their orientations gradually from planar to pyramidal ones. The difference is that in the present reaction the lone-pair orbital bends automatically in the most favorable direction without any subsidiary optimization in the calculations.

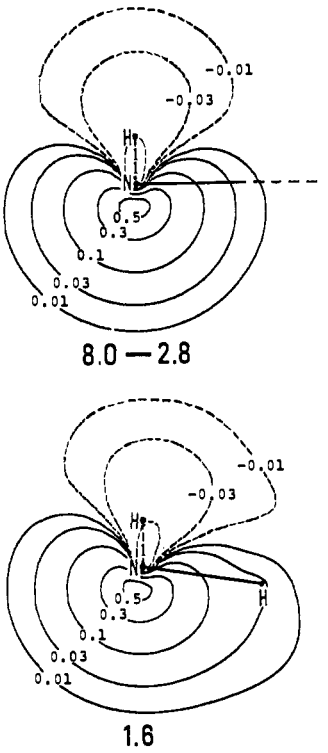

Figure 7. The lone-pair LMO maps. The contour values are given in au, while the N-H distances are in Å unit.

Summary

In this study, we have given the force and density analysis for the radical reaction process $NH_2 + H \rightarrow NH_3$ on the basis of the ESF theory. The results of the present study may be summarized as follows.

(1) Using the density difference, weighted density, and LMO contour maps, we confirmed the electron cloud preceding and the weighted density preceding in the reaction process. These precedings are just the origins of the AD and EC(H-N) forces, which are the most important driving forces of the reaction.

(2) In the initial stage of the reaction, the electron cloud preceding in the atomic region (i.e., the inward polarization of the atomic electron density) is dominant as found for the long-range forces between two neutral atoms in S states.[3b,9a,32] The resultant AD force gives the predominant contribution to the driving force. However, the stabilization energy due to this AD force is small.

(3) In the intermediate stage, the electron cloud preceding occurs as a flow of electron density into the N-H overlap region from the region behind the approaching H nucleus. The electron density accumulated in the N-H region gives a large attractive EC(H-N) force. This EC(H-N) force is the dominant driving force of the reaction in this stage and gives a predominant contribution to the stabilization energy (or the heat of the reaction).

(4) In the last stage, the repulsive EGC force between the undershielded nuclei increases rapidly and terminates the reaction.

(5) The addition of the polarization function on the H atoms is important to improve the H-F force. Although the polarization function has improved all of the AD, EC, and EGC forces, it is especially important for obtaining the AD force.

Acknowledgment. We acknowledge Dr. K. Ishida for the use of the MCSCF program (Y4/CB02) and Dr. S. Kato for the LMO program. We also express our appreciation to the Data Processing Center of Kyoto University for the use of the FACOM 230-75 computer. Part of this study has been generously supported by Scientific Research Grants from the Ministry of Education (155310, 175444, and 139012).

References and Notes

(1) B. M. Deb, *Rev. Mod. Phys.*, **45**, 22 (1973).
(2) B. M. Deb, Ed., "The Force Concept in Chemistry", to be published.
(3) (a) H. Hellmann, "Einführung in die Quanten Chemie", Deuticke, Vienna, 1937; (b) R. P. Feynman, *Phys. Rev.*, **56**, 340 (1939).
(4) R. F. W. Bader and A. K. Chandra, *Can. J. Chem.*, **46**, 953 (1968).
(5) A. K. Chandra and R. Sunder, *Mol. Phys.*, **22**, 369 (1971).
(6) (a) H. Nakatsuji, *J. Am. Chem. Soc.*, **95**, 345, 354, 2084 (1973); (b) H. Nakatsuji and T. Koga in ref 2, Chapter 4.
(7) H. Nakatsuji, T. Kuwata, and A. Yoshida, *J. Am. Chem. Soc.*, **95**, 6894 (1973).
(8) H. Nakatsuji, *J. Am. Chem. Soc.*, **96**, 24, 30 (1974).
(9) (a) H. Nakatsuji and T. Koga, *J. Am. Chem. Soc.*, **96**, 6000 (1974); (b) T. Koga and H. Nakatsuji, *Theor. Chim. Acta*, **41**, 119 (1976); *Chem. Phys.*, **16**, 189 (1976).
(10) K. Fukui, S. Kato, and H. Fujimoto, *J. Am. Chem. Soc.*, **97**, 1 (1975).
(11) K. Fukui, "Theory of Orientation and Stereoselection", Springer-Verlag, West Berlin, 1970.
(12) L. A. Curtiss, C. W. Kern, and R. L. Matcha, *J. Chem. Phys.*, **63**, 1621 (1975).
(13) T. Berlin, *J. Chem. Phys.*, **19**, 208 (1951).
(14) (a) A. K. Chandra and K. L. Sebastian, *Chem. Phys. Lett.*, **41**, 593 (1976); (b) *Mol. Phys.*, **31**, 1489 (1976).
(15) R. F. W. Bader and G. A. Jones, *Can. J. Chem.*, **39**, 1253 (1961); **41**, 2251 (1963).
(16) A brief review of such investigations has been given in ref 8.
(17) A. Veillard and E. Clementi, *Theor. Chim. Acta*, **7**, 133 (1967).

(18) C. Edmiston and K. Ruedenberg, *Rev. Mod. Phys.*, **35**, 457 (1963).
(19) For example, see L. Salem and E. B. Wilson, Jr., *J. Chem. Phys.*, **36**, 3421 (1962); L. Salem and M. Alexander, *ibid.*, **39**, 2994 (1963).
(20) G. G. Hall, *Philos. Mag.*, **6**, 249 (1961).
(21) A. C. Hurley, *Proc. R. Soc. London, Ser. A*, **226**, 170, 179, 193 (1954); P.-O. Lowdin and B. Pullmann, Ed., "Molecular Orbitals in Chemistry, Physics, and Biology", Academic Press, New York, N.Y., 1964.
(22) See for example, B. Roos and P. Siegbahn, *Theor. Chim. Acta*, **21**, 368 (1971).
(23) K. Ruedenberg, *Rev. Mod. Phys.*, **34**, 326 (1962). See also C. W. Wilson and W. A. Goddard, *Theor. Chim. Acta*, **26**, 195 (1972); W. A. Goddard and C. W. Wilson, *ibid.*, **26**, 211 (1972).
(24) G. Herzberg, "Molecular Spectra and Molecular Structure. III. Electronic Spectra and Electronic Structure of Polyatomic Molecules", Van Nostrand, Princeton, N.J., 1966.
(25) K. Ishida, K. Kondo, and T. Yonezawa, *J. Chem. Phys.*, **66**, 2883 (1977).
(26) In the MCSCF calculations, we have used the two-by-two rotation technique of Hinze (ref 27) for $R < 1.6$ Å and the modified single-vector diagonalization technique (with $\lambda = 0.1$) of Wood and Veillard (ref 28) for $R \geq 1.6$ Å.
(27) J. Hinze, *J. Chem. Phys.*, **59**, 6424 (1973).
(28) M. H. Wood and A. Veillard, *Mol. Phys.*, **26**, 595 (1973).
(29) R. F. Stewart, *J. Chem. Phys.*, **52**, 431 (1970).
(30) A. R. Hoy, I. M. Mills, and G. Strey, *Mol. Phys.*, **24**, 1265 (1972).
(31) H. B. Schlegel, S. Wolfe, and F. Bernardi, *J. Chem. Phys.*, **63**, 3632 (1975). They used a different equilibrium geometry, N–H = 0.995 Å and ∠HNH = 113.7°, which is the optimum geometry for the 4-31G basis set.
(32) J. O. Hirschfelder and M. A. Eliason, *J. Chem. Phys.*, **47**, 1164 (1967); J. O. Hirschfelder and W. J. Meath, *Adv. Chem. Phys.*, **12**, 3 (1967).
(33) (a) R. F. W. Bader, W. H. Henneker, and P. E. Cade, *J. Chem. Phys.*, **46**, 3341 (1967); (b) R. F. W. Bader and A. D. Bandrauk, *ibid.*, **49**, 1653 (1968); R. F. W. Bader, I. Keaveny, and G. Runtz, *Can. J. Chem.*, **47**, 2308 (1969); (c) R. F. W. Bader, I. Keaveny, and P. E. Cade, *J. Chem. Phys.*, **47**, 3381 (1967); (d) P. E. Cade, R. F. W. Bader, W. H. Henneker, and I. Keaveny, *ibid.*, **50**, 5313 (1969).
(34) Note that the weighted density represents only the electronic contribution to the force. The preceding of the centroid of the weighted density was also found at the equilibrium structure, but the attractive force due to this preceded density cancels out the nuclear repulsion as seen in Figure 3.
(35) For the free state, the lone-pair LMO is the so-called sp^2 lone pair of the NH_2 radical, while in the final NH_3 molecule it is the so-called sp^3 lone pair. However, we found that the contours of the lone-pair LMOs are essentially superimposable at all range of the reaction except for the direction of their axes.

Through-Bond Interaction of Two Mutually Perpendicular π Systems. A Comparison with Spiroconjugation[1]

Peter Bischof, Rolf Gleiter,* and Rudolf Haider

Contribution from the Institut für Organische Chemie der Technischen Hochschule Darmstadt, D-61 Darmstadt, West Germany. *Received March 3, 1977*

Abstract: It is postulated that two mutually perpendicular π systems can interact effectively via the σ bonds of a cyclobutane ring. This interaction leads to the opposite splitting as predicted for spiroconjugation. Several model systems are discussed.

If two mutually perpendicular π systems π(A) and π(A′) are linked together as shown in Figure 1a, the associated π orbitals interact through space. This phenomenon has been studied theoretically[2,3] as well as by experimental techniques[2,4-6] and is called spiroconjugation. The controlling factors are evident from perturbation arguments.[7] To result in sizable changes of the electronic structure of such molecules due to spiroconjugation, the following two conditions must therefore be met: (a) The interaction term $\beta^{\mu\nu}_{\text{spiro}} = \langle \pi^{\mu}(A)|H|\pi^{\nu}(A')\rangle$ must be large. (b) The interacting orbitals $\pi^{\mu}(A)$ and $\pi^{\nu}(A')$ should have degenerate (or nearly degenerate) basis orbital energies. The latter condition leads to the expectation that spiroconjugation is most important for systems in which the formal π fragments π(A) and π(A′) are identical. Such molecules have D_{2d} symmetry if π(A) and π(A′) are mutually perpendicular, planar π systems. Within this symmetry, the total representation of π orbitals factorizes into three sets of A_2, B_1, and E symmetry. In other words, π orbitals with an even number of nodal planes split into an A_2 and a B_1 combination, while π orbitals with an odd number of nodal planes remain degenerate, since $\beta^{\mu\nu}_{\text{spiro}}$ is 0 for symmetry reasons. Two points should be noted: (1) π orbitals have one nodal plane to begin with, and (2) the a_2 and b_1 orbitals will remain strictly σ–π orthogonal, while the e levels will mix with appropriate σ orbitals.[8] Theory[2,3] supports the expectation that the "in phase" combinations B_1 will be stabilized while the "out of phase" combinations A_2 are destabilized. This is illustrated in Figure 1a.

Apart from these considerations, the effects of spiro conjugation will be determined mainly by the size of the interaction matrix elements $\beta^{\mu\nu}_{\text{spiro}}$. Within the Mulliken approximation[9] (i.e., $\beta^{\mu\nu}_{\text{spiro}} = kS^{\mu\nu}$), this term will remain small throughout, since the overlap integrals $S^{\mu\nu}$ between the coupling atomic orbitals (i.e., the terminal p orbitals of π(A) and π(A′)) are small in magnitude, typically about 0.025.[3]

The disadvantage of the small overlap integral can be overruled by introducing "relay orbitals". With this we mean orbitals which enforce the interaction. Obviously a cyclobutane ring offers perfect conditions as a through-bond coupling partner: (1) the symmetry of the corresponding molecules is maintained and (2) cyclobutane has high-lying occupied and low-lying unoccupied orbitals of appropriate symmetry.

It should be noted that there is no intrinsic difference between the general case of a through-bond interaction[10] of two π orbitals and the specific case discussed here. The one σ bond in the former is replaced by a four-membered ring in the latter. This way the π bonds are locked into a rigid perpendicular arrangement as in spiro compounds. The four-membered ring as a link is unique insofar as replacing it by any other monocyclic system leads to steric difficulties or a reduction of symmetry (the π bonds are not perpendicular any more). It is known that, if such through-bond interaction[10] is dominant, it results in a reversal of the orbital sequence. This is indicated in Figure 1b.

To discuss the effects of this postulated through-bond spiroconjugation, we will refer to the four typical model systems **1**, **2**, **3**, and **4** shown in Scheme I and compare them with the through-space analogues **1′**, **2′**, **3′**, and **4′**. Furthermore, we wish to illustrate the parallelism and difference to be expected between the two types of systems. The extension to systems where the systems π(A) and π(A′) are no longer equivalent is given later on.

"Relay Orbitals"

As mentioned before, we consider the cyclobutane ring in the tricyclic compounds (Figure 1b) as a relay which enforces

0002-7863/78/1500-1036$01.00/0